small NANO MICRO

Biomaterials

Conducting-Polymer Nanotubes Improve Electrical Properties, Mechanical Adhesion, Neural Attachment, and Neurite Outgrowth of Neural Electrodes

Mohammad Reza Abidian, Joseph M. Corey, Daryl R. Kipke, and David C. Martin*

An in vitro comparison of conducting-polymer nanotubes of poly(3,4-ethylenedioxythiophene) (PEDOT) and poly(pyrrole) (PPy) and to their film counterparts is reported. Impedance, charge-capacity density (CCD), tendency towards delamination, and neurite outgrowth are compared. For the same deposition charge density, PPy films and nanotubes grow relatively faster vertically, while PEDOT films and nanotubes grow more laterally. For the same deposition charge density (1.44 C cm^{-2}), PPy nanotubes and PEDOT nanotubes have lower impedance ($19.5 \pm 2.1\,k\Omega$ for PPy nanotubes and $2.5 \pm 1.4\,k\Omega$ for PEDOT nanotubes at 1 kHz) and higher CCD (184 ± 5.3 mC cm^{-2} for PPy nanotubes and 392 ± 6.2 mC cm^{-2} for PEDOT nanotubes) compared to their film counterparts. However, PEDOT nanotubes decrease the impedance of neural-electrode sites by about two orders of magnitude (bare iridium $468.8 \pm 13.3\,k\Omega$ at 1 kHz) and increase capacity of charge density by about three orders of magnitude (bare iridium 0.1 ± 0.5 mC cm^{-2}). During cyclic voltammetry measurements, both PPy and PEDOT nanotubes remain adherent on the surface of the silicon dioxide while PPy and PEDOT films delaminate. In experiments of primary neurons with conducting-polymer nanotubes, cultured dorsal root ganglion explants remain more intact and exhibit longer neurites ($1400 \pm 95\,\mu m$ for PPy nanotubes and $2100 \pm 150\,\mu m$ for PEDOT nanotubes) than their film counterparts. These findings suggest that conducting-polymer nanotubes may improve the long-term function of neural microelectrodes.

Keywords:
- bioelectronics
- conducting polymers
- nanotubes
- neural electrodes
- neurite

[*] Dr. M. R. Abidian, Prof. D. R. Kipke
Department of Biomedical Engineering, The University of Michigan
1101 Beal Ave., Ann Arbor, MI 48109 (USA)
E-mail: mabidian@umich.edu
Prof. J. M. Corey
Department of Neurology, The University of Michigan
Ann Arbor, MI 48109 (USA)
Prof. D. C. Martin[+]
Department of Materials Science and Engineering, Macromolecular Science and Engineering, and Biomedical Engineering
Ann Arbor, MI 48109 (USA)
[+] Present address: Karl W. Boer and Chair Materials Science and Engineering, The University of Delaware 201C Dupont Hall, Newark, DE 19716 (USA)

DOI: 10.1002/smll.200901868

1. Introduction

Interfacing electronics directly with the human nervous system holds considerable promise for allowing closed-loop control of neural prostheses by disabled patients.[1] While multielectrode recordings have become routine[2,3] in animal neurophysiology and have been used in humans,[1] robust and stable long-term recording and stimulation remain a challenge. To obtain reliable and successful chronic signals, the electrode must be biocompatible, have low impedance, and high charge-injection density. Current neural electrodes such as microwires[4,5] and microfabricated electrode arrays[2,6] suffer from high initial impedance and low charge-transfer capacity because of their small-feature geometry.[7] Furthermore, cellular reactive responses increase the electrode–tissue

impedance due to insertion trauma and the chronic foreign-body reaction induced by tethering, micromotion, and device biocompatibility.[8,9] Although several strategies have been conducted to improve the electrical properties[10–14] and reactive tissue responses of neural electrodes,[8,15–17] the long-term efficacy of these devices is still a challenge.

In the physiologic environment, bioelectric signals are carried in the form of ionic currents. The purpose of a microelectode is to transduce these biological signals to and from electronic signals.[18] Conducting polymers such as poly(pyrrole) (PPy) and poly(3,4-ethylenedioxythiophene) (PEDOT) have both electronic and ionic conductivity and have been recently considered for bioelectronic[19,20] and biomedical applications,[21,22] especially neuronal cell signaling[23] and neural interfaces.[13,24–26] These materials can have electrical properties similar to semiconductors and metals while their mechanical properties are relatively soft, similar to conventional polymers. Their response to electrochemical oxidation or reduction can produce a reversible change in conductivity, color, wettability, and volume.[27–32] Among conducting polymers, PPy and PEDOT have been reported to decrease electrode impedance and increase charge-injection capacity as compared to metal sites of similar geometric area.[11–14] Neuronal and muscle cell interactions and cytotoxicity have been extensively investigated for conducting polymers.[33–35] Langer et al. examined the biocompatibility of dissociated primary cerebral cortical cells cultured on PPy samples that had been doped with polystyrene sulfonate. They showed that PPy had favorable reactive tissue responses through attenuation of glial responses and enhanced integration of neuronal processes.[36] Schmidt et al. reported that micropatterned PPy created topographical cues for neuronal cells and had an effect on axon orientation.[34] Wang and co-workers showed that nanoscale topography on polyaniline (PANi) films might contribute to the change in hydrophilicy of the surface, which induced the attachment and proliferation of PC-12 pheochromocytoma cells on PANi films.[37]

Building on previous work demonstrating that electrospun nanofibers promote adhesion and also guide developing and regenerating neurites,[38–40] we performed a study to investigate whether a similar nanoscale morphology of conducting polymers would have similar effects on neurite outgrowth. In addition, we investigated how templated electrospun nanofibers affected the adherence and deposition of PPy and PEDOT on the surface of electrode sites. In vitro electrochemical impedance spectroscopy (EIS) and cyclic voltammetry (CV) measurements showed that PEDOT film and PEDOT nanotube coatings had lower impedance and higher charge-capacity density (CCD) than PPy film and PPy nanotube coatings deposited with the same deposition charge density. We found that PPy nanotubes and PEDOT nanotubes remained adherent to the surface of electrodes during cyclic voltammetry (CV) while PPy films and PEDOT films delaminated. We also examined the effect of nanoscale topography on primary dorsal root ganglion explant (DRG) attachment, and neurite outgrowth. Although all substrates supported neurite outgrowth in a radial direction away from the ganglia, these novel results confirmed that randomly oriented PPy nanotubes and PEDOT nanotubes promoted neurite outgrowth. DRG cells had better attachment, less branches, and longer neurites on PEDOT nanotubes. These are the first reported data of primary neurons growing on electrodeposited conducting-polymer nanotubes.

2. Results and Discussion

Initially, we fabricated conducting-polymer coatings and examined their morphology. As shown in Figure 1, PPy nanotubes and PEDOT nanotubes were formed on eight-channel "Michigan" neural electrode sites (Center for Neural Communication Technology) by a templating method.[11] Briefly, the fabrication process on the surface of a neural electrode (Figure 1a and b) includes: 1) electrospinning of poly (L-lactic acid) (PLLA) nanofibers on the surface of neural electrode (Figure 1c and d), 2) electrochemical deposition of conducting polymers on the electrode sites and around the PLLA nanofibers as a function of deposition time (Figure 1e and f), and 3) removing PLLA template nanofibers by dissolving them in dichloromethane (Figure 1g and h).

Figure 2 shows scanning electron microscopy (SEM) images of PPy film, PEDOT film, PPy nanotubes, and PEDOT nanotubes in a three-dimensional (3D) view (Figure 2a,d,g,j), a top view at a lower magnification (Figure 2b,e,h,k), and a top view at a higher magnification (Figure 2c,f,i,l). Conducting polymers were deposited on the surface of iridium electrode sites (1250 μm^2) with an applied charge density of 1.44 C cm^{-2}. This charge density corresponds to the minimum impedance of

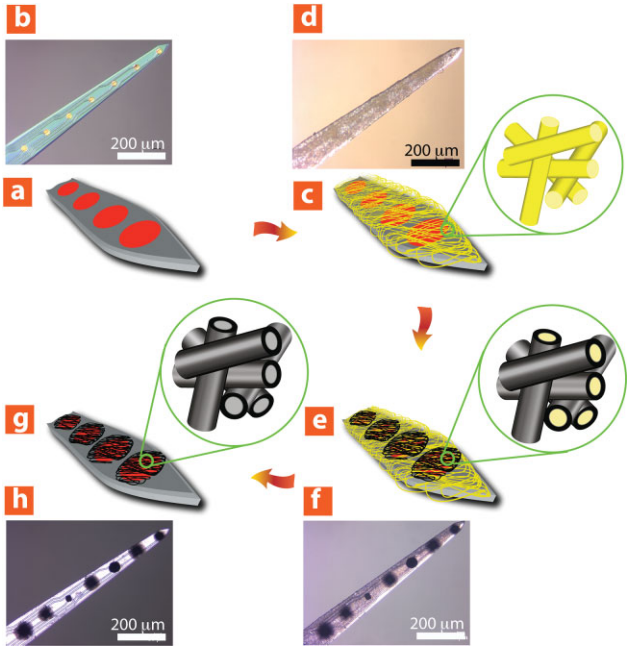

Figure 1. Schematic illustration and optical micrographs of fabrication process of conducting-polymer nanotubes on the surface of neural microelectrodes. a,b) Before surface modification, c,d) electrospinning of PLLA nanofiber templates on the neural microelectrode, e,f) electrochemical deposition of conducting polymer (PEDOT) on the electrode sites and around electrospun PLLA nanofiber templates as a function of deposition time (deposition charge density from 0.24 C cm^{-2} to 2.88 C cm^{-2}), g,h) dissolving away of electrospun PLLA nanofiber templates and formation of conducting-polymer nanotubes.

NANO MICRO small

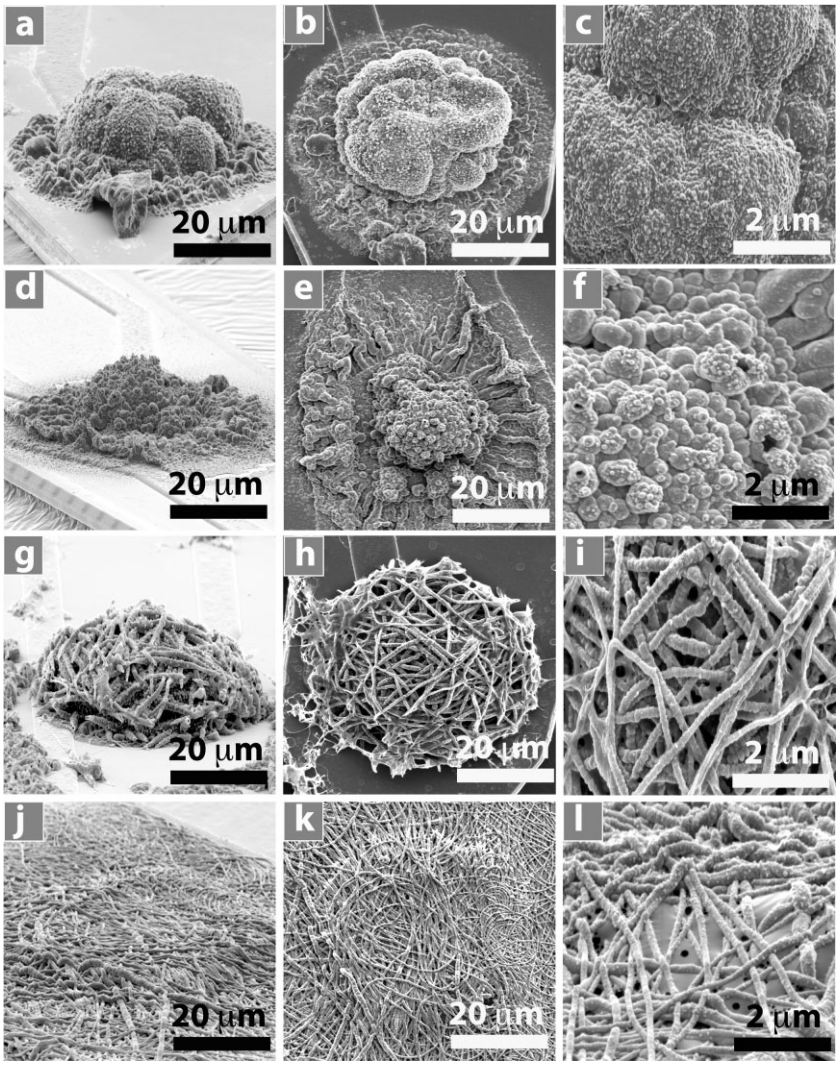

Figure 2. SEM image of electropolymerized nanostructured conducting polymers on the electrode sites with deposition charge density of 1.44 C cm^{-2}. 3D view: a) PPy film, d) PEDOT film, g) PPy nanotubes, j) PEDOT nanotubes. Top view: b) PPy film, e) PEDOT film, h) PPy nanotubes, k) PEDOT nanotubes. High-magnification top view: c) PPy film, f) PEDOT film, i) PPy nanotubes, l) PEDOT nanotubes.

these coatings at 1 kHz,[12] which is the relevant frequency typical of neuronal action potentials. The outer diameter of PPy nanotubes and PEDOT nanotubes was 130 ± 12 nm and 110 ± 8 nm respectively with inner diameter of 97 ± 8 nm (diameter of PLLA nanofibers). We examined the outgrowth diameter of the conducting polymers as a function of deposition charge density from 0.24 C cm^{-2} to 2.88 C cm^{-2} for PPy film, PEDOT film, PPy nanotubes, and PEDOT nanotubes (Figure 3a). The outgrowth diameter increased with increasing deposition charge density. SEM images revealed enhanced growth of conducting polymer on the non-conductive silicon dioxide layer close to the circular edge of electrodes, presumably due to high charge density around the edges.[41] Figure 3c and d shows extended growth of PEDOT and PPy nanotubes on the silicon dioxide with a deposition charge density of 1.44 C cm^{-2}. As shown in Figure 3a, c, and d the outgrowth diameter of PEDOT and PPy nanotubes was 100 ± 5.3 μm and 60 ± 3.5 μm ($p < 0.0001$) respectively, clearly beyond the 40-μm diameter of electrode sites and onto the surrounding silicon dioxide. The greater growth of PEDOT compared to PPy on the silicon dioxide might be explained by formation of higher concentration of EDOT radical cations around the edges of electrode. Other potential explanations are the differences in the wettability and charge of pyrrole and EDOT radicals.[42]

We also measured the total thickness of PPy and PEDOT nanotube assemblies as a function of deposition charge density. The thickness increased for both types of conducting polymer nanotubes as the deposition charge density increased (Figure 3b). By increasing deposition charge density from 0.24 C cm^{-2} to 2.88 C cm^{-2}, it can be seen that the thickness increased from 2.2 ± 1.2 μm to 30 ± 2.5 μm for PPy nanotubes and from 2.5 ± 1.4 μm to 18 ± 2.1 μm for PEDOT nanotubes.

CV measurements were carried out by applying a scanning voltage from −0.9 V to 0.5 V at a scan rate 100 mV s^{-1} for 5 cycles on 32 total electrode sites coated with PPy film, PEDOT film, PPy nanotubes, and PEDOT nanotubes (8 each) that were prepared with a deposition charge density of 1.44 C cm^{-2}. It was observed that the extended growth of PPy film and PEDOT film on the silicon dioxide started delaminating (Figure 4a–f) while PPy nanotubes and PEDOT nanotubes remained firmly attached to silicon dioxide (Figure 4g and h). The delamination of films was seen in 8 of 8 substrates for each polymer and on 0 of 8 nanotube substrates for each polymer (PPy and PEDOT). Conducting polymers have the ability to actuate (change volume) due to the mass transport during oxidation and reduction processes such as CV. When ions and/or solvent enter the polymer it expands and when they exit it contracts.[29,43,44] This volume change might be the primary mechanism for the delamination of PPy and PEDOT films from the electrode shank, presumably due to poor adhesion properties of electrodeposited conducting-polymer film on the silicon dioxide surrounding the iridium electrode sites. In contrast with PPy and PEDOT films, the PPy and PEDOT nanotubes stayed attached to the silicon dioxide, presumably because they were more porous and softer than the films and therefore less likely to build up internal strain during actuation.

To better characterize the delamination, we measured the delamination height as the maximum distance between the delaminated film and the surface of the neural electrodes for each sample (Figure 4c, d, and f). The delamination height was 3.7 ± 1.3 μm for PPy film and 13.4 ± 2.5 μm for PEDOT film (±Stdv, $n = 8$). More delamination of the PEDOT film was observed than for the PPy film on the edges of electrode sites

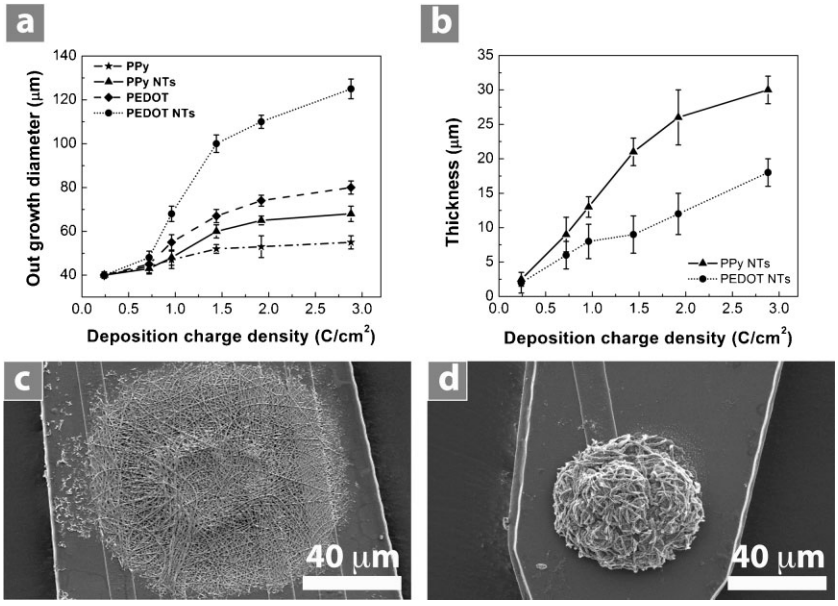

Figure 3. a) Conducting-polymer outgrowth diameter as a function of deposition charge density, PPy film (stars), PPy nanotubes (triangles), PEDOT film (diamonds), and PEDOT nanotubes (circles). b) Thickness of PPy nanotubes (triangles) and PEDOT nanotubes (circles) as a function of deposition charge density. It can be seen that the thickness increased from 2.2 ± 1.2 μm to 30 ± 2.5 μm for PPy nanotubes and from 2.5 ± 1.4 μm to 18 ± 2.1 μm for PEDOT nanotubes by increasing deposition charge density from 0.24 C cm^{-2} to 2.88 C cm^{-2}. Data are shown for ± standard deviation ($n = 10$). c) SEM image of PEDOT nanotube outgrowth on silicon dioxide showing diameter outgrowth of 100 ± 5.3 μm. d) SEM image of PPy nanotube outgrowth on silicon dioxide showing diameter outgrowth of 60 ± 3.5 μm. PEDOT and PPy nanotube were electropolymerized on electrode sites with a deposition charge density of 1.44 C cm^{-2}.

($p < 0.0001$). The difference in the height of delamination between the PEDOT and PPy films might be explained by greater rigidity of PEDOT perhaps due to blocking the β-position of the heterocyclic ring and the formation of α–β linkages during polymerization of EDOT monomer.[45]

Despite delamination of the conducting-polymer film edges from the silicon dioxide, SEM images showed that PPy and PEDOT films were intact and there were no cracks on the surface of conducting-polymer films after CV. Impedance spectroscopy and CCD measurements of delaminated PPy and PEDOT films revealed that there were no significant changes in the impedance and CCD of the polymer films before and after delamination. These results suggest that despite the observed delamination of the edge of the PPy and PEDOT films, these films remained intact and adhered to the iridium sites.

Cui et al. investigated the stability of deposited PEDOT films on platinum electrodes for chronic stimulation under biphasic pulse current at 0.35 mC cm^{-2} at 50 Hz for a period of time up to two weeks. They reported that delamination of PEDOT film was seen on ≈23% of electrodes during electrical stimulation and depended on the amount of deposited PEDOT.[40] While our delamination was more extensive, there are three important differences between the two studies. First, our electrodes were iridium while those of Cui and Zhou were platinum. Second, the delamination that we observed was on the silicon dioxide, on which the conducting-polymer films grew in an extended fashion. Third, the total charge density passed through the conducting polymers during our CV measurements was about two orders of magnitude higher than that used to electrically stimulate electrodes in the study by Cui and Zhou. Although high electrochemical stability of deposited PEDOT films was reported after tens of CV cycles [46], the results in vivo are not yet known.

Figure 5 shows SEM images of PPy nanotubes electrochemically polymerized on the electrode sites as a function of applied charge density from 0.24 C cm^{-2} to 2.88 C cm^{-2}. These results show that PPy tends to create nanotubes that are more extended in the vertical direction, where PEDOT grows more in the lateral direction, for the same deposition charge density. This ability to control the lateral and vertical dimensions may make it possible to optimize the extent of interaction with the tissue, the distortion during insertion, and the adhesion of the polymer film to the substrate.

Figure 6a shows electrochemical impedance spectroscopy of electropolymerized PPy film, PEDOT film, PPy nanotubes, and PEDOT nanotubes deposited with an applied charge density of 1.44 C cm^{-2}. Both PEDOT film and PEDOT nanotubes had lower impedance across the frequency range due to higher electrical conductivity of PEDOT than PPy.[12,28,47] However, PEDOT nanotubes exhibited lower impedance than PEDOT film. This can be explained by the increasing effective surface area during nanotube formation (Figure 2). The initial impedance of bare iridium sites was 468.8 ± 13.3 kΩ at 1 kHz, which decreased to 28.3 ± 2.6 kΩ for PPy film, 19.5 ± 2.1 kΩ for PPy nanotubes, 10.8 ± 1.8 kΩ for PEDOT film, and 2.5 ± 1.4 kΩ for PEDOT nanotubes. These results demonstrate superiority of PEDOT nanotubes for neural recordings and stimulations whereas the low-impedance electrode tissue interface is essential.[48] The phase plot of the impedance spectroscopy (Figure 6b) showed that both the uncoated and coated electrodes were capacitive in the low-frequency range (<10 Hz). The phase angle of PEDOT film and PEDOT nanotubes were close to the uncoated electrode at around 80–90°, which showed they were more capacitive than PPy film and PPy nanotubes. The phase angle dramatically decreased for coated electrodes in the frequency range of 10–100 Hz, especially for PEDOT nanotubes, to ≈5°. PEDOT nanotubes were almost purely resistive at 1 kHz (≈0°) in comparison to the bare iridium electrode (uncoated), which was much more capacitive (≈55°). These results show that PEDOT nanotubes act as a capacitive material for frequencies > 1 kHz and as a Faradaic (resistive) material for frequencies <1 kHz for neural stimulation and recording.

CV was used to explore the CCD for conducting polymers that were deposited with an applied charge density of

NANO MICRO small

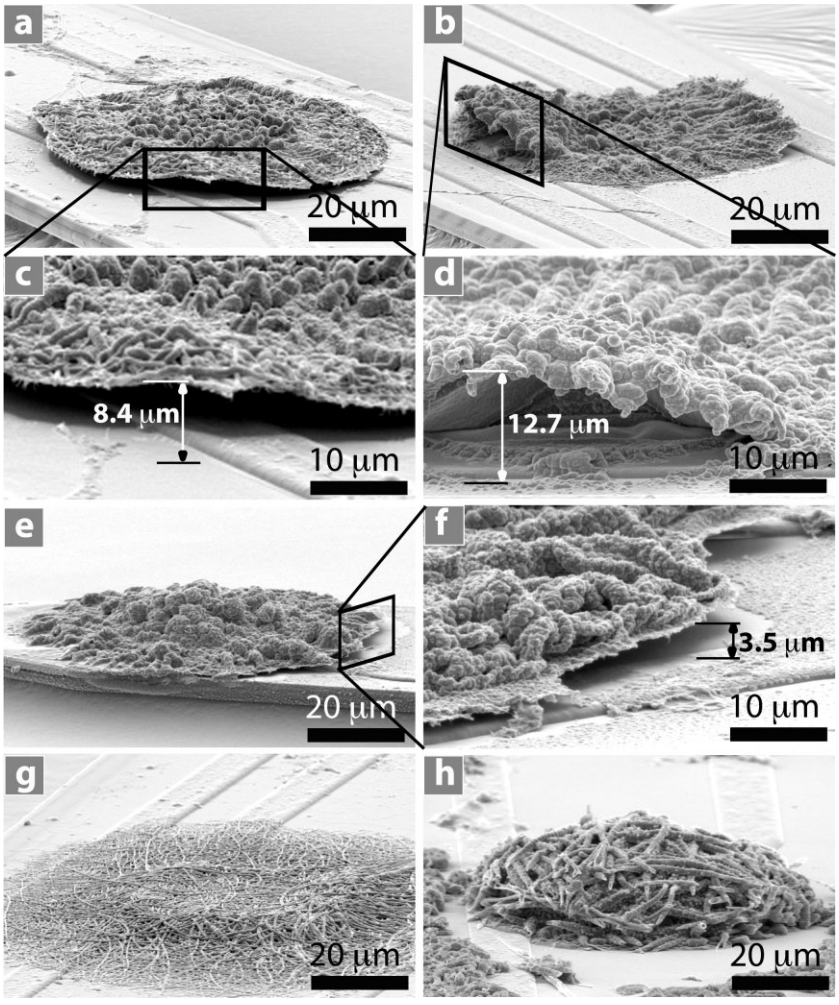

Figure 4. SEM images of conducting polymers after CV measurement on neural electrode: a–d) PEDOT film, e-f PPy film on neural electrode showing delamination on the edge of polymer film. c) Higher-magnification image of (a). d) Higher-magnification image of (b). f) Higher-magnification image of (e). g) PEDOT nanotubes. h) PPy naotubes. PPy nanotubes and PEDOT nanotubes remained firmly attached to the neural electrode after CV measurement. The delamination height was measured as shown in (c), (d), and (f). The delamination height was 3.7 ± 1.3 μm for PPy film and 13.4 ± 2.5 μm for PEDOT film (± Stdv, $n = 8$). More delamination of PEDOT film was observed than for PPy film on the edges of electrode sites ($p < 0.0001$). PEDOT and PPy films and nanotubes were electropolymerized on the electrode site with deposition charge density of 1.44 C cm^{-2}. CV measuerement was carried out by applying scanning voltage from −0.9 V to 0.5 V with scan rate 100 mV s^{-1} for 5 cycles.

1.44 C cm^{-2} (Figure 6c). The surface area under the CV curve is proportional to the CCD of a particular coating material that can transfer during one cycle of CV. The CCD of bare iridium increased significantly for all of the conducting polymers; however, CV results showed that PEDOT could transfer more charge than PPy. The CCD increased from 0.1 ± 0.5 mC cm^{-2} (bare iridium) to 160 ± 8.3 mC cm^{-2} for PPy film, 184 ± 5.3 mC cm^{-2} for PPy nanotubes, 240 ± 9.4 mC cm^{-2} for PEDOT film, and 392 ± 6.2 mC cm^{-2} for PEDOT nanotubes. It was also observed that the CCD of PPy nanotubes increased from 125 ± 3.2 mC cm^{-2} to 625 ± 6.5 mC cm^{-2} with increasing deposition charge density from 0.24 C cm^{-2} to 2.88 C cm^{-2} (Figure 6d). A threshold charge injection density is required to generate neural excitation; however, there is a limit for charge injection density, which causes damage to the neural tissue.[48] Although the charge injection capability of PEDOT for neural stimulation has been briefly reported,[40,49] these CCD results suggest that PEDOT nanotube coatings could be useful for small microelectrodes, which would be suitable for both stimulation and single-unit recording from small neurons.[13,26]

To evaluate the biocompatibility of conducting polymers to neural tissue, primary DRG explants were cultured on PPy and PEDOT films and nanotubes. After collagen coating, DRG was grown for three days, then fixed and stained for neurofilament. DRG explants successfully attached and grew neurites on all conducting polymer substrates. All substrates supported neurite outgrowth in a radial direction away from the ganglia (Figure 7a–d). On visual inspection of all substrates, neurites appeared qualitatively longer on PEDOT than on PPy. Neurites also appeared longer on both conducting-polymer nanotubes compared to their film counterparts. Measuring the neurite length confirmed this finding (1400 ± 95 for PPy nanotubes and 2100 ± 150 μm for PEDOT nanotubes) and with PEDOT nanotubes having the longest neurites and PPy film having the shortest neurites (600 ± 40 μm; Figure 7g).

Neurite morphology also differed among the different polymer surfaces. On both PPy film and PPy nanotubes neurites were not only shorter than on their PEDOT film and PEDOT nanotubes, they appeared comparatively thicker and more branched (Figure 7e), while those on both forms of PEDOT (PEDOT film and PEDOT nanotubes) were thinner and exhibited less branching (Figure 7f). Neurites on PPy appeared to aggregate, or fasciculate, more than on PEDOT. There appear to be fewer and more branched neurites on PPy film than on PPy nanotubes. The ganglia themselves also behaved differently on the two materials. On PEDOT, ganglia appear to have clearly delineated capsules (Figure 7b and d), while capsules around ganglia on PPy are not as easily observed (Figure 7a and c). On PPy, cell bodies appeared to separate from the rest of the ganglia and migrate away from its center.

These results show that electrochemically deposited PPy and PEDOT are compatible with neural tissue and these materials play a role in the extent of neurite growth. This makes it the second in vitro study to show the compatibility of PEDOT, especially PEDOT nanotubes, with growing neurons, after another demonstrating excellent growth of primary cortical neurons.[49] Our in vitro experiments were conducted simultaneously with separate in vivo experiments showing that

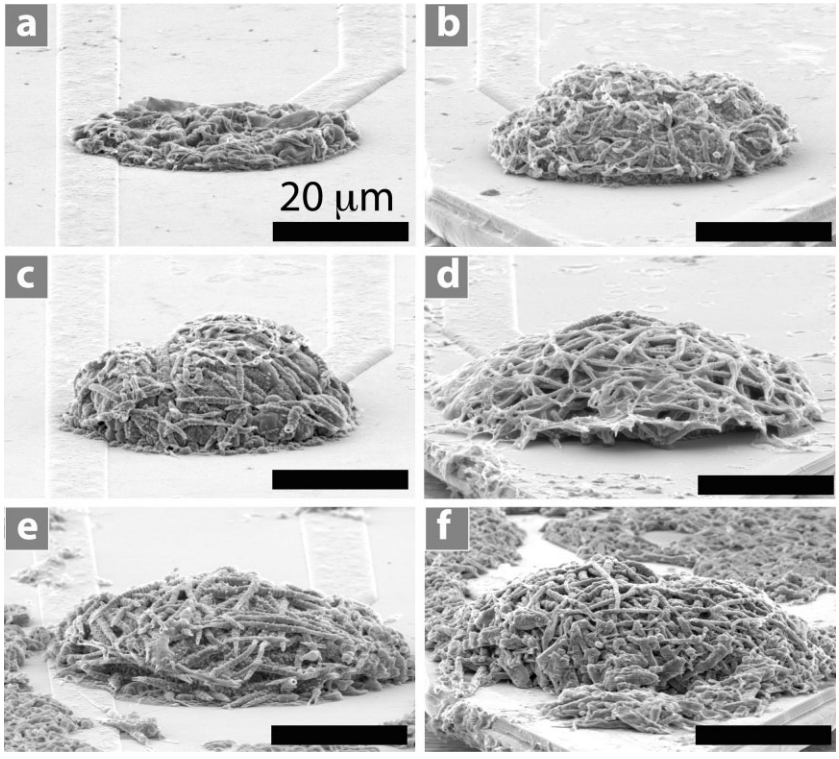

Figure 5. SEM images of electropolymerized PPy nanotubes on neural microelectrode sites as a function of deposition charge density. a) 0.24 C cm^{-2}, b) 0.72 C cm^{-2}, c) 0.96 C cm^{-2}, d) 1.44 C cm^{-2}, e) 1.92 C cm^{-2}, and f) 2.88 C cm^{-2}. It can be seen that the thickness of the PPy nanotube layer increased from 2.2 ± 1.2 μm to 30 ± 2.5 μm. These SEM images demonstrate that PPy nanotubes tend to grow more in the vertical direction.

PEDOT improves quality of recording signals.[26,50] PPy has been more extensively tested, including in vitro experiments with olfactory cells,[51] cortical neurons, and glia[36,52,53] and demonstrating the ability of PPy to electrically stimulate neurite outgrowth.[25] It has also been tested in vivo in scaffolds for nerve regeneration[54,55] and in cortex for its compatibility with neural probes.[36] The morphology of DRG neurites appears highly dependent on the topography of the surface. The highly branched neurite growth on PPy is unusual for DRG explants, the neurites of which grow essentially straight on glass or tissue-culture plastic.[56] This pattern of neurite outgrowth might be explained by differences in charge, wettability, and surface roughness between PPy and PEDOT. Certainly, the more linear neurite growth observed on PPy nanotubes and PEDOT nanotubes is consistent with linear nanostructures that guide neurites such as aligned electrospun nanofibers without overlying PEDOT.[38,39,57]

3. Conclusions

We have reported the superiority of conducting-polymer nanotubes for surface modification of implantable neural electrodes, as compared to dense films. We investigated the effect of nanotube morphology on the attachment of PPy and PEDOT on the surface of electrode sites. We showed that PPy nanotubes and PEDOT nanotubes remained adherent on the surface of electrode during CV while PPy film and PEDOT film delaminated. The delamination of PEDOT film was more than PPy film, presumably due to the higher rigidity of PEDOT. These findings raise several questions to be addressed in future longevity studies. First, even though PPy and PEDOT nanotubes survive 5 cycles of CV, would they delaminate after more? Second, would the same results we have observed here in vitro be seen in vivo? Third, if conducting-polymer films or nanotubes delaminate in vivo, would they eventually degrade into particles that may adversely affect the overall tissue response? Electrochemical impedance spectroscopy and CV measurements demonstrated that PPy nanotubes and PEDOT nanotubes had lower impedance (19.5 ± 2.1 kΩ for PPy nanotubes and 2.5 ± 1.4 kΩ for PEDOT nanotubes at 1 kHz) and higher CCD (184 ± 5.3 mC cm^2 for PPy nanotubes and 392 ± 6.2 mC cm^{-2} for PEDOT nanotubes) compared to their film counterparts. However, PEDOT nanotubes decreased the impedance of neural electrode sites by about two orders of magnitude (bare iridium 468.8 ± 13.3 kΩ at 1 kHz) and increased capacity of charge density by about three orders of magnitude (bare iridium 0.1 ± 0.5 mC cm^{-2}). We also examined the effect of nanoscale topography on attachment and neurite outgrowth of DRG explants. Although all substrates supported neurite outgrowth in a radial direction away from the ganglia, our results demonstrated that PPy nanotubes and PEDOT nanotubes promoted neurite outgrowth. In summary, DRG cells had better attachment and less branched and longer neurites on PEDOT nanotubes (2100 ± 150 μm). These results suggest that nanoscale surface topography might have more influence in cell functions such as adhesion and proliferation. Coupled with the previously demonstrated controlled drug release of conducting-polymer nanotubes[11] this study paves the way for ''smart'' recording/stimulation electrodes, which can precisely deliver neurotrophic factors to induce neurons to grow towards the electrodes.

4. Experimental Section

Materials: High-molecular-weight poly(L-lactic acid) (PLLA, RESOMER L210) with inherent viscosity of 3.3–4.3 dL g^{-1} was purchased from Boehringer Ingelheim Pharma GmbH & Co. (KG, Germany). 3,4-ethylenedioxythiophene (EDOT, BAYTRON M) with molecular weight 142.17 g mol^{-1} was received from H.C. Starck Inc. (Newton, MA). Phosphate buffered saline (PBS, pH = 7.4) was purchased from Mediatech Inc. The pyrrole monomer (Py), collagen I, and lithium perchlorate (LiClO4) were purchased from Sigma–Aldrich. Neurobasal was prepared from Invitrogen.

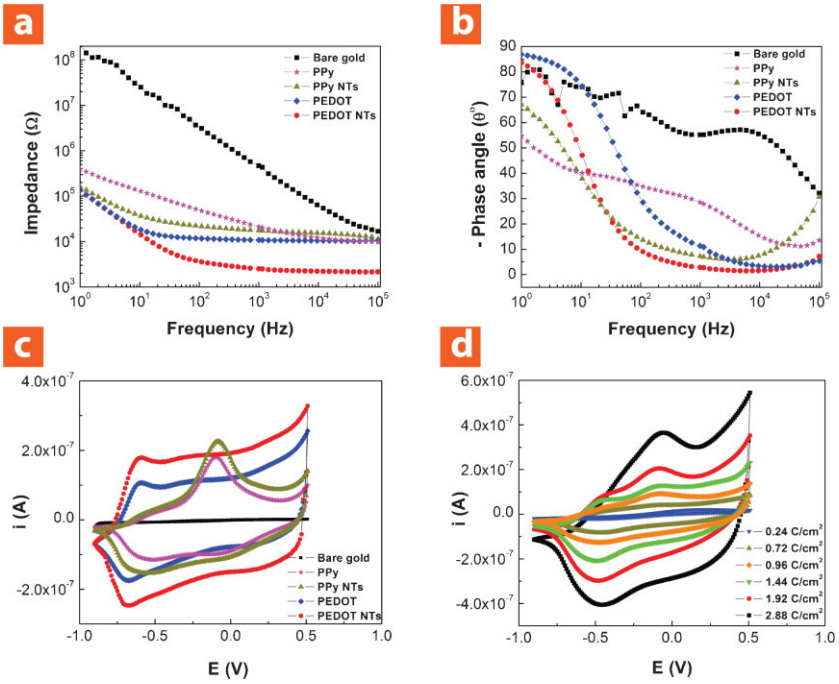

Figure 6. Electrical properties of neural microelectrodes modified with nanostructured conducting polymers. a) Bode plot of electrochemical impedance spectroscopy over a frequency range of 1–10^5 Hz; the initial impedance of bare iridium was 468.8 ± 13.3 kΩ at 1 kHz, which decreased to 28.3 ± 2.6 kΩ for PPy film, 19.5 ± 2.1 kΩ for PPy nanotubes, 10.8 ± 1.8 kΩ for PEDOT film, and 2.5 ± 1.4 kΩ for PEDOT nanotubes. b) Phase plot of electrochemical impedance spectroscopy over a frequency range of 1–10^5 Hz showing that both the uncoated and coated electrodes were capacitive in the low-frequency range (<10 Hz). PEDOT nanotubes were almost purely resistive at 1 kHz (≈0°) in comparison with bare iridium electrode (uncoated), which was much more capacitive (≈55°). c) CV; the potential was swept from −0.9 to 0.5 V at a scan rate of 100 mV s^{-1}. The CCD increased from 0.1 ± 0.5 mC cm^{-2} (bare iridium) to 160 ± 8.3 mC cm^{-2} for PPy film, 184 ± 5.3 mC cm^{-2} for PPy nanotubes, 240 ± 9.4 mC cm^{-2} for PEDOT film, and 392 ± 6.2 mC cm^{-2} for PEDOT nanotubes. Bare iridium (squares), PPy film (stars), PPy nanotubes (triangles), PEDOT film (diamonds), and PEDOT nanotubes (circles). Conducting polymers were deposited with an applied charge density of 1.44 C cm^{-2}. d) CV for PPy nanotubes electropolymerized with a deposition charge density from 0.24 C cm^{-2} to 2.88 C cm^{-2}. CCD of PPy nanotubes increased from 125 ± 3.2 mC cm^{-2} to 625 ± 6.5 mC cm^{-2} with increasing deposition charge density from 0.24 C cm^{-2} to 2.88 C cm^{-2}.

Selenium, hydrocortisone, beta-estradiol, apo-transferrin, and L-glutamine were obtained from Fisher Scientific Company. Rabbit anti-neurofilament was purchased from Chemicon (Temecula, CA).

Electrochemical deposition of conducting polymers: The electrochemical process was performed on individual electrode sites of eight-channel acute neural miroelectrodes with 1250-μm^2 iridium recording sites by an Autolab PGSTAT-12 (EcoChemie, Utrecht, Netherlands) in galvanostatic mode with a conventional two-electrode configuration at room temperature. Conducting-polymer deposition was carried out in a 0.01 M EDOT and 0.1 M $LiClO_4$ (or in a 0.1 M Py and 0.1 M $LiClO_4$) aqueous solution at a current density of 0.5 mA cm^{-2}. Conducting polymers were deposited on total of 40 electrode sites (10 electrode sites for each: PPy film, PPy nanotubes, PEDOT film, and PEDOT nanotubes) with deposition charge density of 1.44 C cm^{-2}. In another set up, the amount of PPy and PEDOT was controlled by the total applied charge density passed during polymerization (0.24–2.88 C cm^{-2}). The working and sensing electrodes were connected to the electrode site. The reference and counter electrode were connected to a platinum wire within the EDOT/$LiClO_4$ and Py/$LiClO_4$ solutions.

Electrochemical impedance spectroscopy: An Autolab PGSTAT-12 and Frequency Response Analyzer software (Eco Chemie B.V., Netherlands) were used to record impedance spectra of the electrode sites. A solution of 0.1 M phosphate buffer solution (PBS, pH = 7) was used as an electrolyte in a three-electrode cell. The working electrode was connected to the electrode site through a connector. The counter electrode was connected to a platinum foil that was placed in a glass container. An Ag/AgCl reference electrode and the neural microelectrode tip were immersed in glass container of electrolyte. An AC sinusoidal signal of 5 mV in amplitude was used to record the impedance over a frequency range of 1–10^5 Hz.

Cyclic voltammetry: CV was performed using an Autolab PGSTAT-12 instrument in a three-electrode configuration as described earlier. A scan rate of 100 mV s^{-1} was used and the potential on the working electrode was swept between −0.9 to 0.5 V. All the potentials are reported versus the Ag/AgCl reference electrode. Before each CV curve was recorded, several cycles were swept to insure that the conducting polymer had reached a stable state. The GPES software (EcoChemie, Utrecht, Netherlands) was used to estimate the total CCD during one cycle of CV.

Primary neuron culture: Before culture, substrates were coated with collagen I (Sigma) solution, at a concentration of approximately 100 μg mL^{-1} in 0.1 M acetic acid. Dorsal root ganglia (DRG) were plucked from the spinal cords of embryonic day-15 Sprague-Dawley rat embryos and placed directly on the substrate in a minimal amount of media. The culture medium consisted of Neurobasal (Invitrogen) with B27 supplement (Gibco BRL) with the following additives: 30 nM selenium, 10 nM hydrocortisone, 10 nM beta-estradiol, 10 mg L^{-1} apo-transferrin, and 2 μM L-glutamine. A small amount of calf serum (up to 5%) was added to promote better explant adhesion and outgrowth.

Immunocytochemistry of DRGs: Following culture, DRG were fixed in 4% paraformaldehyde for 15–30 min and stored in 0.1 M sodium phosphate buffer. Samples were soaked for 15 min in 1% goat serum and 2% non-fat dry milk to block non-specific binding and with 0.05% Triton-X-100 to permeabilize the cells. Rabbit anti-neurofilament (Chemicon, Temecula, CA) was used to label neurons. A Leica MZFL III stereo dissecting fluorescent microscope was used for imaging DRG explants.

Neurite length measurement: MetaMorph 7 software (Molecular Devices Corporation, Sunnyvale, CA) was used to determine the average longest neurite length. To determine the longest neurite length, 30–60 neurite from each DRG were

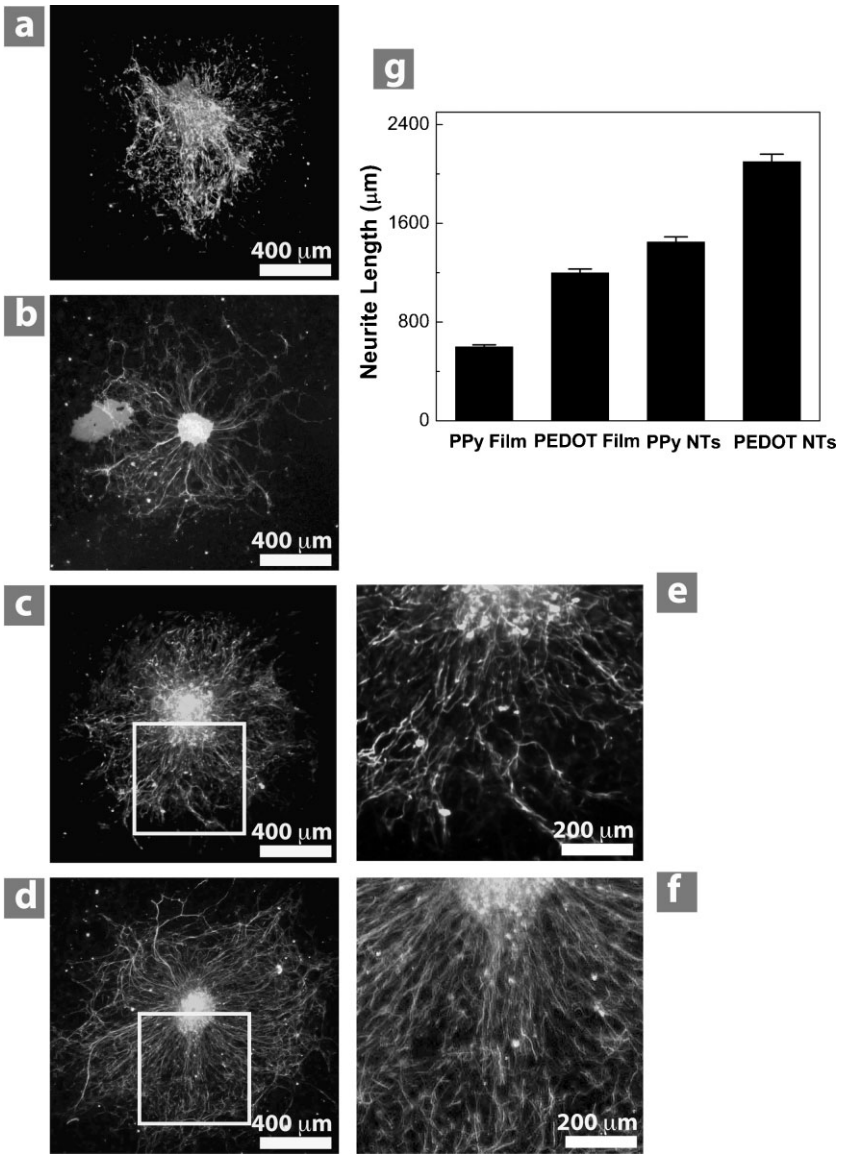

Figure 7. DRG explants cultured on conducting-polymer films and nanotubes. Ganglia on PPy film (a) and PPy nanotubes (c) degraded and had shorter and more branched neurites than PEDOT film (b) and PEDOT nanotubes (d), respectively. The extent of branching is best observed at higher magnification of PPy nanotubes (e) and PEDOT nanotubes (f). Conducting-polymer nanotubes produced longer neurites than their corresponding films, with PEDOT nanotubes producing the longest neurites overall (g). Column height represents the mean while error bars reflect the standard error of the mean for 10 neurites per condition ($n = 10$).

selected and the 10 longest were averaged. The length measured for each neurite was the distance between end of neurite and DRG body radially. Statistical analysis of these data was carried out using a one-way ANOVA test using Prism software (www.graphpad.com).

Acknowledgements

The authors thank Katherine B. Mycek for assistance with explant culture and imaging, Dr. Sheereen Majd and Prof. Michael Mayer for assistance with fluorescence imaging of DRGs and neurite length measurement, Eugene Dariush Daneshvar, Paras Patel, and Nick Langhals for comments on the manuscript. The authors acknowledge the University of Michigan Center for Neural Communication Technology (CNCT), Army Research Office MURI (Contract Number W911NF-06-1-0218, Proposal Number 50376-LS-MUR), NIH-K08-EB003996 (JMC), The NIH-NINDS-NO1-NS-1- 2338, and a Rackham Pre-doctoral Fellowship through the Rackham School of Graduate Studies. M.R.A. and D.C.M. have invention disclosures and patent applications related to these materials pending with the University of Michigan Office of Technology Transfer and the U. S. Patent and Trademark Office.

[1] L. R. Hochberg, M. D. Serruya, G. M. Friehs, J. A. Mukand, M. Saleh, A. H. Caplan, A. Branner, D. Chen, R. D. Penn, J. P. Donoghue, *Nature* **2006**, *442*, 164–171.
[2] D. R. Kipke, R. J. Vetter, J. C. Williams, J. F. Hetke, *IEEE Trans. Neural Syst. Rehab. Eng.* **2003**, *11*, 151–155.
[3] M. A. L. Nicolelis, D. Dimitrov, J. M. Carmena, R. Crist, G. Lehew, J. D. Kralik, S. P. Wise, *Proc. Natl. Acad. Sci. USA* **2003**, *100*, 11041–11046.
[4] D. H. Hubel, *Science* **1957**, *125*, 549–550.
[5] J. C. Williams, R. L. Rennaker, D. R. Kipke, *Brain Res. Protoc.* **1999**, *4*, 303–313.
[6] P. J. Rousche, R. A. Normann, *J. Neurosci. Meth.* **1998**, *82*, 1–15.
[7] D. A. Robinson, *Proc. IEEE* **1968**, *56*, 1065–1071.
[8] D. H. Szarowski, M. D. Andersen, S. Retterer, A. J. Spence, M. Isaacson, H. G. Craighead, J. N. Turner, W. Shain, *Brain Res.* **2003**, *983*, 23–35.
[9] V. S. Polikov, P. A. Tresco, W. M. Reichert, *J. Neurosci. Meth.* **2005**, *148*, 1–18.
[10] K. J. Otto, M. D. Johnson, D. R. Kipke, *IEEE Trans. Biomed. Eng.* **2006**, *53*, 333–340.
[11] M. R. Abidian, D. H. Kim, D. C. Martin, *Adv. Mater.* **2006**, *18*, 405–409.
[12] M. R. Abidian, D. C. Martin, *Biomaterials* **2008**, *29*, 1273–1283.
[13] M. R. Abidian, D. C. Martin, *Adv. Funct. Mater.* **2009**, *19*, 573–585.
[14] X. Y. Cui, D. C. Martin, *Sens. Actuators B* **2003**, *89*, 92–102.
[15] W. Shain, L. Spataro, J. Dilgen, K. Haverstick, S. Retterer, M. Isaacson, M. Saltzman, J. N. Turner, *IEEE Trans. Neural Syst. Rehab. Eng.* **2003**, *11*, 186–188.
[16] L. Kam, W. Shain, J. N. Turner, R. Bizios, *Biomaterials* **2002**, *23*, 511–515.
[17] D. J. Edell, V. V. Toi, V. M. McNeil, L. D. Clark, *IEEE Trans. Biomed. Eng.* **1992**, *39*, 635–643.
[18] G. T. A. Kovacs, in *Enabling Technologies for Cultured Neural Networks*, (Eds: D. A. Stenger, T. M. McKenna), Academic Press, London, UK **1994**, 121–165.

[19] M. Berggren, A. Richter-Dahlfors, *Adv. Mater.* **2007**, *19*, 3201–3213.
[20] G. Wallace, G. Spinks, *Soft Matter* **2007**, *3*, 665–671.
[21] N. K. Guimard, N. Gomez, C. E. Schmidt, *Prog. Polym. Sci.* **2007**, *32*, 876–921.
[22] E. Smela, *Adv. Mater.* **2003**, *15*, 481–494.
[23] J. Isaksson, P. Kjall, D. Nilsson, N. D. Robinson, M. Berggren, A. Richter-Dahlfors, *Nat. Mater.* **2007**, *6*, 673–679.
[24] R. A. Green, N. H. Lovell, G. G. Wallace, L. A. Poole-Warren, *Biomaterials* **2008**, *29*, 3393–3399.
[25] C. E. Schmidt, V. R. Shastri, J. P. Vacanti, R. Langer, *Proc. Natl. Acad. Sci. USA* **1997**, *94*, 8948–8953.
[26] M. R. Abidian, K. A. Ludwig, T. C. Marzullo, C. R. Martin, D. R. Kipke, *Adv. Mater.* **2009**, *21*, 3764–3770.
[27] R. H. Baughman, *Synth. Met.* **1996**, *78*, 339–353.
[28] L. Groenendaal, G. Zotti, P. H. Aubert, S. M. Waybright, J. R. Reynolds, *Adv. Mater.* **2003**, *15*, 855–879.
[29] E. Smela, O. Inganas, I. Lundstrom, *Science* **1995**, *268*, 1735–1738.
[30] L. B. Xu, W. Chen, A. Mulchandani, Y. S. Yan, *Angew. Chem. Int. Ed.* **2005**, *44*, 6009–6012.
[31] E. Smela, N. Gadegaard, *Adv. Mater.* **1999**, *11*, 953–957.
[32] X. Z. Wang, E. Smela, *J. Phys. Chem. C* **2009**, *113*, 359–368.
[33] L. J. del Valle, F. Estrany, E. Armelin, R. Oliver, C. Aleman, *Macromol. Biosci.* **2008**, *8*, 1144–1151.
[34] N. Gomez, J. Y. Lee, J. D. Nickels, C. E. Schmidt, *Adv. Funct. Mater.* **2007**, *17*, 1645–1653.
[35] S. M. Richardson-Burns, J. L. Hendricks, B. Foster, L. K. Povlich, D. H. Kim, D. C. Martin, *Biomaterials* **2007**, *28*, 1539–1552.
[36] P. M. George, A. W. Lyckman, D. A. LaVan, A. Hegde, Y. Leung, R. Avasare, C. Testa, P. M. Alexander, R. Langer, M. Sur, *Biomaterials* **2005**, *26*, 3511–3519.
[37] H. J. Wang, L. W. Ji, D. F. Li, J. Y. Wang, *J. Phys. Chem. B* **2008**, *112*, 2671–2677.
[38] J. M. Corey, C. C. Gertz, B. S. Wang, L. K. Birrell, S. L. Johnson, D. C. Martin, E. L. Feldman, *Acta Biomater.* **2008**, *4*, 863–875.
[39] J. M. Corey, D. Y. Lin, K. B. Mycek, Q. Chen, S. Samuel, E. L. Feldman, D. C. Martin, *J. Biomed. Mater. Res. A* **2007**, *83*, 636–645.
[40] X. T. Cul, D. D. Zhou, *IEEE Trans. Neural Syst. Rehab. Eng.* **2007**, *15*, 502–508.
[41] G. Jin, C. O. Too, J. Norrish, G. G. Wallace, *International Conference on Science and Technology of Synthetic Metals (ICSM 2002)* Shanghai, **2002**.
[42] *Conjugated Polymers: Theory, Synthesis, Properties, and Characterization* (Eds: T. A. Skotheim, J. R. Reynolds), CRC Press/Taylor & Francis Group, Boca Raton, FL **2007**.
[43] E. W. H. Jager, E. Smela, O. Inganas, *Science* **2000**, *290*, 1540–1545.
[44] W. Lu, A. G. Fadeev, B. H. Qi, E. Smela, B. R. Mattes, J. Ding, G. M. Spinks, J. Mazurkiewicz, D. Z. Zhou, G. G. Wallace, D. R. MacFarlane, S. A. Forsyth, M. Forsyth, *Science* **2002**, *297*, 983–987.
[45] A. R. Hillman, I. Efimov, K. S. Ryder, *J. Am. Chem. Soc.* **2005**, *127*, 16611–16620.
[46] M. Dietrich, J. Heinze, G. Heywang, F. Jonas, *J. Electroanal. Chem.* **1994**, *369*, 87–92.
[47] G. Heywang, F. Jonas, *Adv. Mater.* **1992**, *4*, 116–118.
[48] S. R. Cogan, *Annu. Rev. Biomed. Eng.* **2008**, *10*, 275–309.
[49] T. Nyberg, A. Shimada, K. Torimitsu, *J. Neurosci. Meth.* **2007**, *160*, 16–25.
[50] K. A. Ludwig, J. D. Uram, J. Y. Yang, D. C. Martin, D. R. Kipke, *J. Neural Eng.* **2006**, *3*, 59–70.
[51] S. Lakard, G. Herlem, N. Valles-Villareal, G. Michel, A. Propper, T. Gharbi, B. Fahys, *Biosens. Bioelectron.* **2005**, *20*, 1946–1954.
[52] W. R. Stauffer, X. T. Cui, *Biomaterials* **2006**, *27*, 2405–2413.
[53] R. Wadhwa, C. F. Lagenaur, X. T. Cui, *J. Controlled Release* **2006**, *110*, 531–541.
[54] X. Wang, X. Gu, C. Yuan, S. Chen, P. Zhang, T. Zhang, J. Yao, F. Chen, G. Chen, *J. Biomed. Mater. Res. A* **2004**, *68*, 411–422.
[55] Z. Zhang, M. Rouabhia, Z. Wang, C. Roberge, G. Shi, P. Roche, J. Li, L. H. Dao, *Artif. Organs* **2007**, *31*, 13–22.
[56] K. Isahara, M. Yamamoto, *Dev. Brain Res.* **1995**, *84*, 164–178.
[57] Y. T. Kim, V. K. Haftel, S. Kumar, R. V. Bellamkonda, *Biomaterials* **2008**, *29*, 3117–3127.

Received: October 3, 2009
Published online: January 13, 2010